"dimerization" are of the same magnitude as the exchange rate of VO_4^{3-}.

Further ^{18}O studies are anticipated to give information concerning the extent of oligomerization and the nature of the ions in the region between VO_4^{3-} and $V_{10}O_{28}^{6-}$.

Acknowledgment. The author wishes to express appreciation to the Research Council, University of Missouri, for partial support of this work and to K. Giese for independent experimental verification.

Registry No. VO_4^{3-}, 14333-18-7; H_2O, 7732-18-5; $[Co(NH_3)_6]_4(V_2O_7)_3$, 60645-68-3; $[Co(NH_3)_6]VO_4$, 60645-69-4.

References and Notes

(1) M. T. Pope and B. W. Dale, *Q. Rev., Chem. Soc.*, **25**, 527 (1971).
(2) G. Jander and K. F. Jahr, *Z. Anorg. Allg. Chem.*, **212**, 1 (1933).
(3) F. Brito, N. Ingri, and L. G. Sillen, *Acta Chem. Scand.*, **18**, 1557 (1964).
(4) (a) O. W. Howarth and R. E. Richards, *J. Chem. Soc.*, 864 (1965); (b) J. V. Hatton, Y. Saito, and W. G. Schneider, *Can. J. Chem.*, **43**, 47 (1965).
(5) W. P. Griffith and P. J. B. Lesniak, *J. Chem. Soc. A*, 1066 (1969).
(6) A. Gaglani, N. Asting, and W. H. Nelson, *Inorg. Chem.*, **13**, 1715 (1974).
(7) H. T. Evans, *Inorg. Chem.*, **5**, 967 (1966).
(8) M. P. Whittaker, J. Asay, and E. M. Erying, *J. Phys. Chem.*, **70**, 1005 (1966).
(9) R. K. Murmann, *J. Am. Chem. Soc.*, **96**, 7836 (1974).
(10) G. Johnson and R. K. Murmann, submitted for publication in *Inorg. Synth.*
(11) I am indebted to Mr. Ken Giese for these measurements.
(12) P. Souchay and R. Schaal, *Bull. Soc. Chim. Fr.*, 842 (1950).
(13) F. Brito and N. Ingri, *An. R. Soc. Esp. Fis. Quim., Ser. B*, **56**, 165 (1960).
(14) L. Newman, W. J. LaFleur, F. J. Brousaides, and A. M. Ross, *J. Am. Chem. Soc.*, **80**, 4491 (1958).
(15) H. Gamsjäger and P. Baertschi, *Helv. Chim. Acta*, **55**, 2154 (1972).
(16) R. H. Betts and R. H. Voss, *Can. J. Chem.*, **48**, 2035 (1970).
(17) R. K. Murmann, *J. Phys. Chem.*, **71**, 974 (1967).
(18) H. Goff and R. K. Murmann, *J. Am. Chem. Soc.*, **93**, 6058 (1971).
(19) R. T. Sanderson, "Inorganic Chemistry", Reinhold, New York, N.Y., 1956, p 136.
(20) R. K. Murmann, *J. Am. Chem. Soc.*, **93**, 4184 (1971).
(21) R. H. Holyer and H. W. Baldwin, *Can. J. Chem.*, **45**, 413 (1967).
(22) K. Giese, M.S. Thesis, University of Missouri, 1976.

Contribution from Lash Miller Chemical Laboratories and Erindale College, University of Toronto, Toronto, Ontario, Canada

Synthesis of Binary Gold Carbonyls, $Au(CO)_n$ (n = 1 or 2). Spectroscopic Evidence for Isocarbonyl(carbonyl)gold, a Linkage Isomer of Bis(carbonyl)gold

D. McINTOSH and G. A. OZIN*

Received March 1, 1976 AIC60160T

The cocondensation reaction of Au atoms with CO/M mixtures (where M = Ne, Ar, Kr, or Xe) at 6–10 K leads to the formation of authentic binary gold carbonyls, $Au(CO)_n$ (where n = 1 or 2). These complexes were characterized using metal and ligand concentration studies, $^{12}C^{16}O/^{13}C^{16}O$/M isotopic substitution, and warm-up experiments in conjunction with matrix infrared and uv–visible spectroscopy as well as isotope frequency and intensity calculations. The infrared data for bis(carbonyl)gold favor a linear, symmetrical $D_{\infty h}$ structure. Detailed investigations of the complexes in inert gas matrices revealed a variety of interesting site effects and matrix-induced frequency shifts. The latter can be rationalized in terms of Buckingham's theory of nonspecific solvent shifts applied to matrix-isolated species. Particularly noteworthy were the unusual vibrational isotope patterns observed for the product formed when gold atoms were deposited with $^{12}C^{16}O/^{13}C^{16}O$, $^{12}C^{16}O/^{12}C^{18}O$, and $^{12}C^{16}O/^{13}C^{18}O$ mixtures. Ten distinct, mixed isotopic molecules containing *nonequivalent* carbonyl ligands were identified. An a priori interpretation of the isotopic shifts was in terms of an isocarbonyl(carbonyl)gold complex, (OC)Au(OC), a linkage isomer of bis(carbonyl)gold. The existence of the linkage isomer is thought to be a consequence of the head-to-tail orientational requirements of the CO molecules in the fccub lattice of crystalline carbon monoxide, rather than an inherent preference for the isocarbonyl isomer. Similar results were obtained in the isomorphous α-N_2 lattice under both high- and low-concentration conditions and lend credence to the idea of a lattice-stabilized isocarbonyl–carbonyl complex. Additional information was obtained from the corresponding uv–visible spectra in Ar/CO and CO matrices, respectively. In this context, the results of extended Hückel molecular orbital calculations proved to be quite helpful for understanding the differences between a symmetrical C-bonded dicarbonyl, an asymmetrical C-bonded dicarbonyl, and an isocarbonyl–carbonyl complex.

Introduction

Since the very early failures to synthesize group 1B carbonyls,[1] the chemistry of zerovalent gold has remained elusive. However, with the recent discovery that group 1B metal atoms are highly reactive toward carbon monoxide at cryogenic temperatures, it has proven possible to synthesize and characterize binary carbonyls of the form $M(CO)_n$ and $M_2(CO)_6$ (M = Cu, Ag; n = 1–3) using matrix-isolation techniques.[2]

We have now extended our earlier studies with Cu and Ag atoms to include Au atoms in an effort to complete our knowledge of the carbon monoxide complexes of the coinage metals. Rather than providing a simple extension of the Cu/CO and Ag/CO systems, the Au/CO reaction products exhibited some chemically intriguing differences.

In brief, only *two* mononuclear carbonyls of gold, $Au(CO)_n$ (n = 1 or 2), could be synthesized in CO/M matrices (M = Ar, Kr, Xe) whereas *three* carbonyls, $M(CO)_m$ (m = 1–3), could be obtained for copper and silver.

Of considerable chemical interest was the discovery that a complex with the spectroscopic characteristics of isocarbonyl(carbonyl)gold, Au(CO)(OC), a linkage isomer of $Au(CO)_2$, could be stabilized in pure CO and N_2 lattices, whereas no compelling evidence was obtained for linkage isomers of the corresponding copper or silver carbonyls.

The following is a detailed account of our investigations.

Experimental Section

Monatomic Au was generated either by directly heating a thin tungsten rod (0.025 in.) around the center of which was wound gold wire (0.005 in.) or by directly heating a tantalum Knudsen cell (wall thickness 0.015 in., orifice diameter 0.010–0.020 in.), the Au being contained in a boron nitride liner (wall thickness 0.010 in.). The gold metal (99.99%) was supplied by Imperial Smelting Co., Toronto. Research grade $^{12}C^{16}O$ (99.99%) was supplied by Matheson of Canada, $^{12}C^{16}O/^{13}C^{16}O$ and $^{12}C^{16}O/^{12}C^{18}O$ isotopic mixtures were supplied by Stohler, Montreal, and $^{12}C^{16}O/^{13}C^{18}O$ mixtures were supplied by Prochem, Summit, N.J. The furnace used for the evaporation of the metal has been previously described.[3] The rate of metal atom deposition was continuously monitored using a quartz crystal microbalance.[4] To obtain quantitative data for Au/CO and Au/CO/M (M = Ne, Ar, Kr, Xe, or N_2) cocondensations, it was necessary to calibrate carefully the rate of deposition of both metal

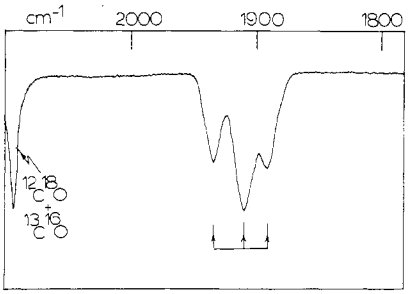

Figure 1. Matrix infrared spectrum of Au atoms deposited into a $^{12}C^{16}O/^{13}C^{16}O/Ne \simeq 1/1/20$ mixture at 6–10 K, showing the presence of $Au(^{12}C^{16}O)_n(^{13}C^{16}O)_{2-n}$ ($n = 0$–2).

and gas onto the sample window as described previously.[5] In the infrared experiments, matrices were deposited on either an NaCl or a CsI plate cooled to 10–12 K by means of an Air Products Displex closed-cycle helium refrigerator or to 6 K by a liquid helium transfer system. Spectra were recorded on a Perkin-Elmer 180 spectrophotometer. Uv–visible spectra were recorded on a standard Unicam SP 8000 instrument in the range 190–700 nm or a Varian Techtron in the range 190–900 nm, the sample being deposited onto an NaCl optical plate cooled to 6–8 K. In the ESR experiments, the sample was deposited onto a sapphire rod (dimensions 1.75 in. × 0.12 in. × 0.04 in.) cooled to 6 K. Using a specially designed telescopic vacuum shroud,[6] the sample could be lowered into an extension quartz tailpiece held in the microwave cavity of a standard Varian E4 spectrometer. ESR spectra were recorded in the range 0–6000 G with microwave powers varied between 0.1 and 10 mW for optimum resolution conditions. In view of the photochemical lability of silver tricarbonyl to the radiation emitted from the Nernst glower,[2] all infrared experiments were conducted with a germanium uv–visible cutout filter placed between the source and the sample.

Results and Discussion

Bis(carbonyl)gold, $Au(CO)_2$. When Au atoms are cocondensed with a $^{12}C^{16}O/Ne = 1/10$ mixture at 6–10 K, a strong absorption is observed at 1935.8 cm^{-1} which is replaced in a $^{12}C^{16}O/^{13}C^{16}O/Ne = 1/1/20$ mixture by a triplet isotope pattern with components at 1935.8, 1909.5, and 1890.6 cm^{-1} having an approximately 1/2/1 intensity ratio (Figure 1). These data establish the product to be $Au(CO)_2$, most probably with a linear, symmetrical structure as predicted theoretically.[18]

The observed and calculated frequencies and intensities for $Au(^{12}C^{16}O)_n(^{13}C^{16}O)_{2-n}$ ($n = 0$–2) based on the Cotton–Kraihanzel force field approximation[19] and isotope intensity sum rules[20] are shown in Table I and are in excellent agreement for the three observed CO stretching modes. Furthermore, the calculations predict that the "missing" $^{12}C^{16}O$ in-phase CO stretching mode is probably not observed because of its inherently low absorbance.

When the reaction is reexamined in $^{12}C^{16}O/Ar = 1/40$ matrices at 6–10 K, a well-resolved doublet is observed at 1926.6 and 1914.8 cm^{-1} compared to the single line observed in $^{12}C^{16}O/Ne$. A higher frequency absorption is also observed at 2039.4 cm^{-1} in Ar/CO matrices which is shown from warm-up and mixed isotope experiments, described later, to belong to gold monocarbonyl (see Figure 2 and Table I).

That the doublet at 1926.6 and 1914.8 cm^{-1} is a case of a matrix multiple-trapping site effect for a dicarbonyl stems from the corresponding $^{12}C^{16}O/^{13}C^{16}O/Ar = 1/1/80$ experiment, which displays a characteristic doublet-of-triplets isotope pattern (Figure 2), consistent with the presence of two slightly different forms of $Au(CO)_2$ (referred to as site 2_1 and 2_2). Geometrically, both forms contain equivalent CO groups but differ presumably in the site perturbation that each senses in the Ar lattice. (The sensitivity of the site effect to the matrix ratio is seen, for example, from a $^{12}C^{16}O/^{13}C^{16}O/Ar = 1/1/20$ experiment which shows the presence of only a single-site, triplet isotope pattern.) Additional support for the dicarbonyl assignment in Ar matrices stems from the results of isotope frequency and intensity calculations shown in Table I.

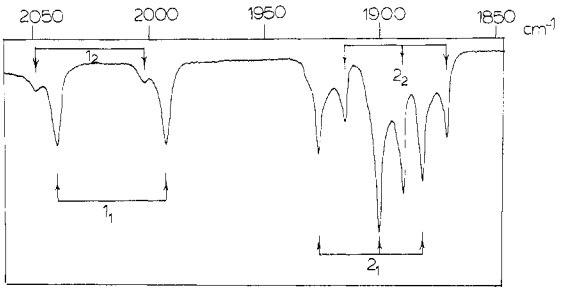

Figure 2. Matrix infrared spectrum of Au atoms deposited into a $^{12}C^{16}O/^{13}C^{16}O/Ar \simeq 1/1/80$ mixture at 6–10 K, showing the presence of $Au(^{12}C^{16}O)_n(^{13}C^{16}O)_{2-n}$ ($n = 0$–2; 2_1 and 2_2 refer to two different matrix sites of the dicarbonyl) and $Au(^{12}C^{16}O)_n(^{13}C^{16}O)_{1-n}$ ($n = 0$–1; 1_1 and 1_2 refer to two different matrix sites of the monocarbonyl).

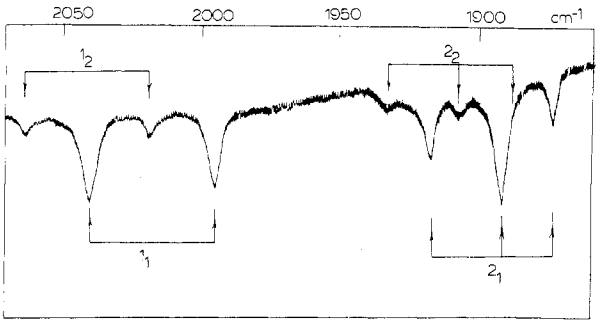

Figure 3. Same case as Figure 2 except that a $^{12}C^{16}O/^{13}C^{16}O/Kr \simeq 1/1/50$ mixture was used.

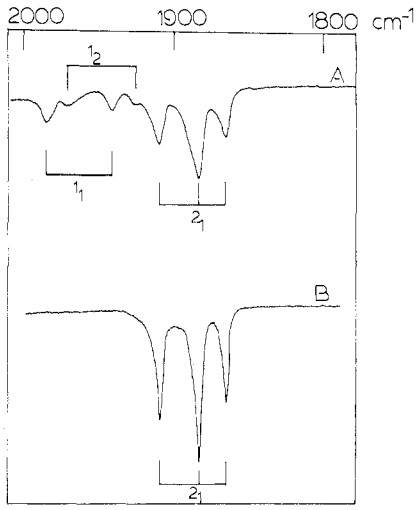

Figure 4. (A) Same case as Figure 2 except that a $^{12}C^{16}O/^{13}C^{16}O/Xe \simeq 1/1/40$ mixture was used. (B) Spectrum recorded after warm-up to 70 K.

Apart from the predicted frequency shifts on passing from Ar to Kr to Xe matrices (see later), the $^{12}C^{16}O/^{13}C^{16}O/Kr = 1/1/50$ and $^{12}C^{16}O/^{13}C^{16}O/Xe = 1/1/40$ infrared spectra show the same basic triplet isotope patterns as seen in Ne and Ar except that a single site for $Au(^{12}C^{16}O)_n(^{13}C^{16}O)_{2-n}$ ($n = 0$–2) in Xe appears to be favored (Figures 3 and 4 and Table I).

An insight into the thermal stability of $Au(CO)_2$ was obtained from warm-up experiments in $^{12}C^{16}O/^{13}C^{16}O/Xe$ matrices which showed the presence of unchanged dicarbonyl

Table I. Observed and Calculated Frequencies and Intensities of Isotopic $Au(^{12}C^{16}O)_n(^{13}C^{16}O)_{2-n}$ (Where $n = 0$–2)

ν		Intensity		
Obsd	Calcd	Obsd	Calcd[a]	Assignment[c]
		Neon		
1890.6	1891.7	8.54	9.56	III (Σ_u^+)
1909.5	1909.5	21.23	18.96	II (Σ^+)
1935.8	1934.7	10.00	10.00	I (Σ_u^+)
N.o.[b]	2046.2	N.o.	0.60	II (Σ^+)
$f_r = 16.18$ mdyn/Å; $f_{rr} = 0.95$ mdyn/Å				
		Krypton		
1871.9	1873.2	9.29	9.56	III (Σ_u^+)
1891.0	1891.0	22.91	19.01	II (Σ^+)
1917.0	1915.8	10.00	10.00	I (Σ_u^+)
N.o.	2034.5	N.o.	0.55	II (Σ^+)
$f_r = 15.93$ mdyn/Å; $f_{rr} = 1.11$ mdyn/Å				
		Xenon		
1865.5	1866.4	8.76	9.56	III (Σ_u^+)
1883.7	1883.7	21.69	18.87	II (Σ^+)
1909.7	1908.7	10.00	10.00	I (Σ_u^+)
N.o.	2009.5	N.o.	0.69	II (Σ^+)
$f_r = 15.67$ mdyn/Å; $f_{rr} = 0.95$ mdyn/Å				
		Argon–Site 1		
1881.2	1882.5	13.77	12.90	III (Σ_u^+)
1900.2	1900.2	22.73	21.99	II (Σ^+)
1926.6	1925.3	10.00	10.00	I (Σ_u^+)
N.o.	2034.0	N.o.	0.72	II (Σ^+)
$f_r = 16.00$ mdyn/Å; $f_{rr} = 1.03$ mdyn/Å				
		Argon–Site 2		
1870.6	1871.5	13.88	12.90	III (Σ_u^+)
1889.6	1889.5	21.36	22.19	II (Σ^+)
1914.8	1914.0	10.00	10.00	I (Σ_u^+)
N.o.	2046.4	N.o.	0.53	II (Σ^+)
$f_r = 16.02$ mdyn/Å; $f_{rr} = 1.22$ mdyn/Å				

[a] The calculated intensities were corrected for an unequal mixture of the isotopic gases $^{12}C^{16}O/^{13}C^{16}O$ with $[^{12}C^{16}O]/[^{13}C^{16}O]$ approximately equal to 0.86. [b] N.o. = not observed. [c] I ≡ $Au(^{12}C^{16}O)_2$; II ≡ $Au(^{12}C^{16}O)(^{13}C^{16}O)$; III ≡ $Au(^{13}C^{16}O)_2$.

at 70 K (Figure 4) at which temperature the xenon matrix was beginning to break up.

In summary, the highest stoichiometry complex formed in CO/M mixtures (M = Ne, Ar, Kr, Xe) is bis(carbonyl)gold, having a linear, symmetrical $D_{\infty h}$ structure (analogous to $Cu(CO)_2$ and $Ag(CO)_2$[2]).

On the other hand, the data obtained in pure $^{12}C^{16}O/^{13}C^{16}O$ and $^{12}C^{16}O/^{13}C^{16}O/N_2$ matrices are quite distinct from those in Ne, Ar, Kr, and Xe matrices and deserve special consideration.

Spectroscopic Evidence for Isocarbonyl(carbonyl)gold, Au(CO)(OC). When gold atoms are cocondensed with pure $^{12}C^{16}O$ at 6–10 K (Au/CO ≤ $1/10^4$ to avoid binuclear complex formation—see, for example, ref 2), the infrared spectrum shows an intense absorption at 1927.7 cm^{-1} together with a weak absorption at 2072 cm^{-1} (Figure 5). In a number of different runs, these two absorptions always appeared with the *same* intensity ratio after deposition and, moreover, retained the same ratio during warm-up experiments (see later), implying that they are associated with a single species. (The weak line at 1904 cm^{-1} is shown from mixed isotopic substitution experiments to be a matrix site effect of the main line at 1927.7 cm^{-1}.)

The stoichiometry and structure of this compound were established from metal concentration and mixed isotopic substitution experiments.

When gold atoms are cocondensed with $^{12}C^{16}O$ at 6–10 K using *high* concentrations of gold (Au/CO ≃ $1/10^2$, to *promote* binuclear complex formation—see ref 2), the infrared

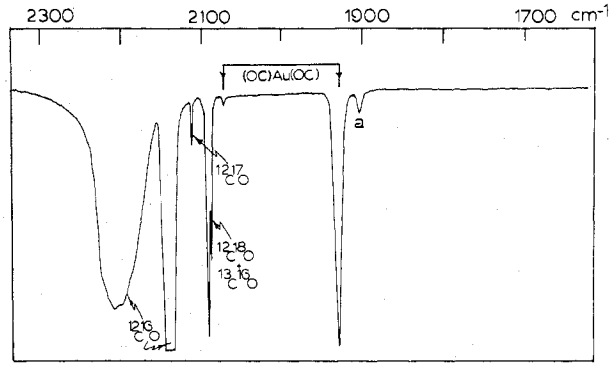

Figure 5. Matrix infrared spectrum of Au atoms deposited with pure $^{12}C^{16}O$ at 6–10 K, showing the two absorptions associated with Au(CO)(OC). The weak line at 1904 cm^{-1} (labeled "a") is shown from mixed isotopic substitution to be a multiple-trapping site effect of Au(CO)(OC).

spectrum was identical with that described above for $Au/^{12}C^{16}O \leq 1/10^4$ except for the growth of a weak, broad line at about 2200 cm^{-1}. The absorbance of this line relative to the line at 1927.7 cm^{-1} was dependent on the Au/CO ratio, implying the presence of a binuclear or higher aggregate complex. On the basis of gold concentration experiments, the species absorbing at 1927.7 cm^{-1} can confidently be assigned to a mononuclear gold carbonyl.

Additional support for the mononuclear formulation stems from preliminary ESR investigations, which show the presence of a complex having spin $I = 1/2$ and axial symmetry.[7]

The stoichiometry with respect to the ligand was established from $Au/^{12}C^{16}O/^{13}C^{16}O \simeq 0.5/10^4/10^4$ experiments, a typical infrared spectrum being shown in Figure 6A and C. The spectrum is best described as a quartet of lines, the components of which have approximately equal intensities.

By employment of long deposition times, the $^{12}C^{16}O/^{13}C^{16}O$ isotopic pattern associated with the weak, high-frequency absorption at 2072 cm^{-1} could also be observed (Figure 6C).

There can be no doubt that the molecule obtained contains two CO groups. However, one is forced to the inescapable conclusion that in a CO matrix the molecule contains *nonequivalent* CO ligands as evidenced by the closely spaced central doublet of the quartet pattern (Figure 6A).

An important clue regarding the exact nature of this complex originated from the analogous $Au/^{12}C^{16}O/^{12}C^{18}O \simeq 0.5/10^4/10^4$ reaction products, the infrared spectrum of which is shown in Figure 6B. Once again we observe an intense quartet pattern, the components of which have roughly equal intensities. However, two features of this spectrum compared to the corresponding $Au/^{12}C^{16}O/^{13}C^{16}O$ spectrum are particularly relevant. First, the closely spaced central doublet has a *smaller* splitting for the $^{12}C^{16}O/^{12}C^{18}O$ mixture (1.8 cm^{-1}) compared to that for the $^{12}C^{16}O/^{13}C^{16}O$ mixture (3.9 cm^{-1}), indicating breakdown of the frequency-factored (Cotton–Kraihanzel[19]) force field. Second, the lowest frequency component of the quartet pattern, corresponding to the presence of the complex containing two $^{13}C^{16}O$ ligands, absorbs at a *lower* frequency (1885.3 cm^{-1}) than the complex containing two $^{12}C^{18}O$ ligands (1887.9 cm^{-1}). This unusual set of circumstances, together with the inequivalence of the CO ligands, would suggest an a priori assignment to an isocarbonyl(carbonyl)gold complex, (OC)Au(OC), which may be construed to be one of the linkage isomers of normal (OC)Au(CO), the latter being obtained in inert-gas matrices. If our isocarbonyl–carbonyl proposal is correct, then the presence of the very weak absorption at 2072 cm^{-1} (Figures 5 and 6C) may depict the isocarbonyl group frequency.

Because of the insensitivity of a Cotton–Kraihanzel force field calculation to the mode of bonding of the carbonyl ligand,

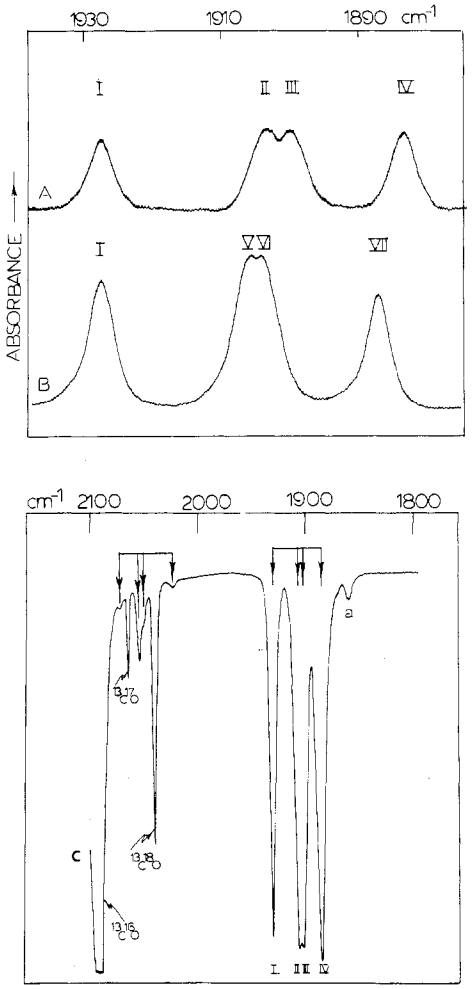

Figure 6. Matrix infrared spectrum of Au atoms deposited with (A) a $^{12}C^{16}O/^{13}C^{16}O \simeq 1/1$ mixture and (B) a $^{12}C^{16}O/^{12}C^{18}O \simeq 1/1$ mixture at 6–10 K, showing the presence of the seven distinct mixed isotopic molecules Au($^{12}C^{16}O$)($^{16}O^{12}C$) (I), Au($^{12}C^{16}O$)($^{16}O^{13}C$) (II), Au($^{13}C^{16}O$)($^{16}O^{12}C$) (III), Au($^{13}C^{16}O$)($^{16}O^{13}C$) (IV), Au($^{12}C^{16}O$)($^{18}O^{12}C$) (V), Au($^{12}C^{18}O$)($^{16}O^{12}C$) (VI), Au($^{12}C^{18}O$)($^{18}O^{12}C$) (VII). Curve C is the same as curve A but with a complete scan after a long deposition time, showing the quartet isotopic pattern associated with the weak, high-frequency absorption at 2072, 2054, 2050, and 2024 cm^{-1} (note that under these conditions, weak absorptions due to trace amounts of free $^{13}C^{17}O$ and $^{13}C^{18}O$ in the commercial $^{12}C^{16}O/^{13}C^{16}O$ mixture were observed in the 2100–2000-cm^{-1} region).

it is necessary in an isocarbonyl–carbonyl situation to include metal–ligand as well as ligand stretching and stretch–stretch interaction force constants.

Using the internal coordinates shown in

$$\overset{r}{O}\equiv\overset{R}{C}-Au-\overset{R'}{O}\equiv\overset{r'}{C}$$

one requires an MVFF composed of ten force constants. In order to obtain a meaningful analysis of the isotopic data, a minimum of ten distinct mixed isotopic molecules is required. From the $^{12}C^{16}O/^{13}C^{16}O$ and $^{12}C^{16}O/^{12}C^{18}O$ experiments, only seven independent isotopic molecules and seven observable frequencies were obtained. By use of a $^{12}C^{16}O/^{13}C^{18}O$ isotopic mixture (Figure 7), three additional molecules and their corresponding frequencies were obtained and thereby yielded our minimal basis set of ten independent isotopic frequencies for (OC)Au(OC) (the isotopic components of the 2072-cm^{-1} absorption could be included in the calculation as four additional constraints).

By employing an initial set of k_{CO} and k_{CO-CO} force constants similar to those for normal (OC)Au(CO) and

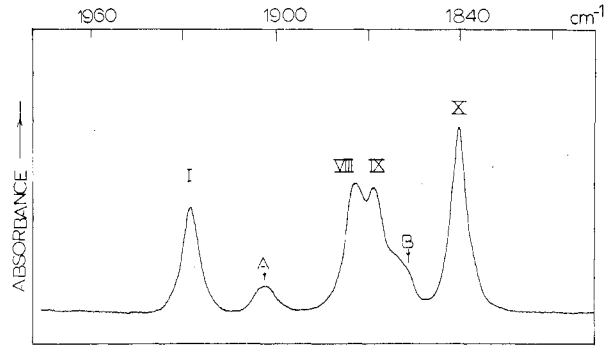

Figure 7. Matrix infrared spectrum of Au atoms deposited into a $^{12}C^{16}O/^{13}C^{18}O = 43/49.7$ mixture at 6–10 K, showing the presence of the four isotopic molecules Au($^{12}C^{16}O$)($^{16}O^{12}C$) (I), Au($^{12}C^{16}O$)($^{18}O^{13}C$) (VIII), Au($^{13}C^{18}O$)($^{16}O^{12}C$) (IX), and Au($^{13}C^{18}O$)($^{18}O^{13}C$) (X). The lines marked A and B arise from the presence of 2.7% $^{13}C^{16}O$ and 4.6% $^{12}C^{18}O$ in the 43.0% $^{12}C^{16}O$/49.7% $^{13}C^{18}O$ isotopic mixture. These give rise to observable quantities of the eight mixed isotopic molecules Au($^{12}C^{16}O$)($^{16}O^{13}C$)/Au($^{13}C^{16}O$)($^{16}O^{12}C$), Au($^{12}C^{16}O$)($^{18}O^{12}C$)/Au($^{12}C^{18}O$)($^{16}O^{12}C$), Au($^{12}C^{18}O$)($^{18}O^{13}C$)/Au($^{13}C^{18}O$)($^{18}O^{12}C$), and Au($^{13}C^{16}O$)($^{18}O^{13}C$)/Au($^{13}C^{18}O$)($^{16}O^{13}C$). Band overlap problems unfortunately prevented the resolution of most of these mixed isotopic molecules.

Table II. Observed and Calculated CO Stretching Frequencies for Ten Isotopically Labeled (OC)Au(OC) Molecules Based on an MVFF Analysis[a]

Freq, cm^{-1}			
Obsd	Calcd[b]	Notation	Assignment
1927.7	1930.0	I	($^{16}O^{12}C$)Au($^{16}O^{12}C$)
1905.4	1907.7	II	($^{16}O^{12}C$)Au($^{16}O^{13}C$)
1901.5	1901.7	III	($^{16}O^{13}C$)Au($^{16}O^{12}C$)
1885.3	1885.3	IV	($^{16}O^{13}C$)Au($^{16}O^{13}C$)
1906.3	1905.5	V	($^{16}O^{12}C$)Au($^{18}O^{12}C$)
1904.5	1904.3	VI	($^{18}O^{12}C$)Au($^{16}O^{12}C$)
1887.9	1886.1	VII	($^{18}O^{12}C$)Au($^{18}O^{12}C$)
1876.5	1876.4	VIII	($^{16}O^{12}C$)Au($^{18}O^{13}C$)
1869.9	1870.1	IX	($^{18}O^{13}C$)Au($^{16}O^{12}C$)
1842.6	1840.3	X	($^{18}O^{13}C$)Au($^{18}O^{13}C$)
2072	2107.7	I	
2054	2087.7	II	
2050	2086.4	III	
2024	2060.6	IV	
	2090.1	V	
	2081.0	VI	
	2057.3	VII	
	2074.9	VIII	
	2065.5	IX	
	2009.0	X	

[a] Best fit force constants (in mdyn/Å; see text for notation): $k_{r'} = 16.22$, $k_R = 1.87$, $k_r = 15.24$, $k_{R'} = 0.99$, $k_{rR} = -0.41$, $k_{rR'} = -0.35$, $k_{rr'} = 1.07$, $k_{RR'} = 0.70$, $k_{Rr'} = -0.06$, $k_{R'r'} = -0.26$. [b] In this analysis, the ten out-of-phase CO stretching modes were used to obtain the best fit between the observed and calculated CO stretching frequencies.

reasonable guesses for the remaining six force constants, we computed best fit frequencies for (OC)Au(OC) and, for completeness (although chemically less acceptable), (OC)Au(CO)*, the latter containing two C-bonded yet *nonequivalent* carbonyl groups. For chemically reasonable sets of optimized force constants, both the isocarbonyl(carbonyl) and bis(carbonyl) (with nonequivalent CO groups) models yielded equally acceptable fits between the observed and calculated isotopic frequencies for all observed modes. This, in part, relates to the spectroscopic nonobservation (above 200 cm^{-1}) and hence exclusion of gold–ligand stretching frequencies in the normal-coordinate calculations.

The results of the isocarbonyl–carbonyl calculations for illustrative purposes are listed in Table II. It is interesting

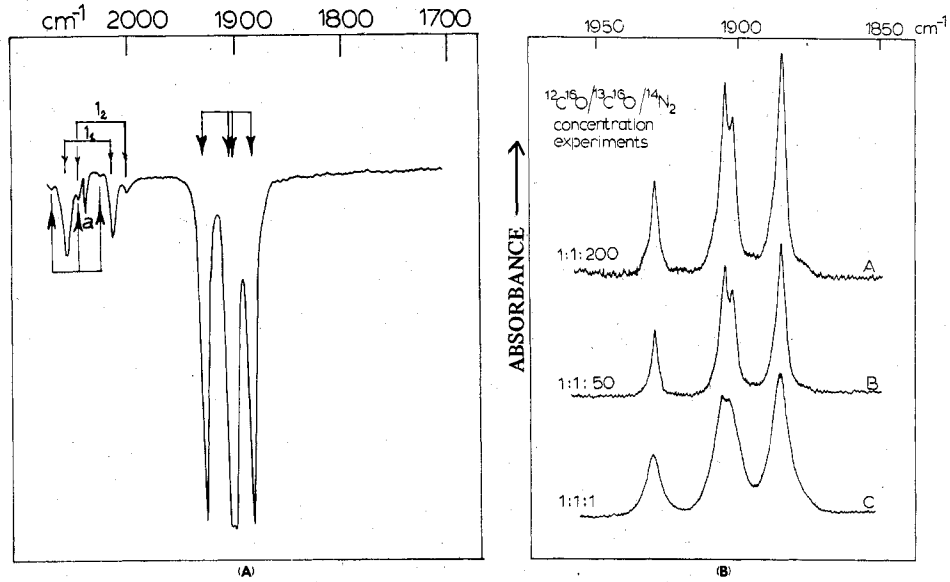

Figure 8. (A) Matrix infrared spectrum of Au atoms deposited with $^{12}C^{16}O/^{13}C^{16}O/N_2 \simeq 1/1/10$ at 10 K, showing the presence of a site-split gold monocarbonyl complex, as well as isocarbonyl(carbonyl)gold ("a" indicates trace amounts of $^{13}C^{18}O$ in the matrix). (B) Same case as (A) but showing the effect of dilution of $^{12}C^{16}O/^{13}C^{16}O$ in N_2: A, 1/1/200; B, 1/1/50; C, 1/1/1.

to note that the calculated values of the gold–carbon and gold–oxygen stretching modes (not shown in Table II) are below 300 cm^{-1}, which would be consistent with our inability to observe these modes even with the carbonyl stretching mode fully absorbing and recorded with 10× ordinate expansions.

If our isocarbonyl–carbonyl proposal is correct, then, to the best of our knowledge, the discovery of isocarbonyl(carbonyl)gold would represent the first case of a complex containing a *terminal* isocarbonyl ligand (bridging O-bonded carbonyls are, of course, well documented—see for example ref 8). [Additional support for the isocarbonyl-carbonyl stems from the uv–visible experiments and from the results in N_2 matrices (see later).]

In view of the formation of normal bis(carbonyl)gold in Ne, Ar, Kr, and Xe matrices, we believe that the stabilization of the linkage isomer isocarbonyl(carbonyl)gold in CO matrices is most likely a consequence of the orientational requirements of the CO molecules in the fccub lattice of crystalline carbon monoxide, preventing the complex from rearranging to the normal bis(carbonyl) isomer. An examination of Au atoms residing in a substitutional site of solid CO reveals that, of the 12 nearest neighbors, only *one* set of two CO molecules is favorably aligned for approximately linear, twofold coordination. Of these two molecules, one is oriented with its carbon end and the other with its oxyen end adjacent to the gold atom. This type of head-to-tail lattice restriction, rather than an inherent preference for the isocarbonyl isomer, may be responsible for the stabilization of (OC)Au(OC).

As a final thought, it is interesting to consider the behavior of Au atoms deposited into a $CO/N_2 = 1/5$ mixture. The infrared spectrum shows the presence of only bis(carbonyl)gold, absorbing at 1927.6 cm^{-1}. Evidence for $Au(CO)(N_2)$ or $Au(N_2)_2$ complexes was not obtained. Our inability to prepare these complexes is consistent with the uv–visible observation of atomic gold in pure N_2 matrices.

Nevertheless it is interesting that the infrared frequency for bis(carbonyl)gold in N_2 matrices is virtually identical with that of the isocarbonyl(carbonyl)gold complex in CO matrices. Moreover, its frequency also lies well off the polarizability–frequency plot shown in Figure 1 (see later).

A typical infrared spectrum of Au atoms cocondensed with a $^{12}C^{16}O/^{13}C^{16}O/N_2 \simeq 1/1/10$ matrix at 10 K is shown in Figure 8A. Aside from some monocarbonyl (see later) absorbing at 2060 cm^{-1} ($Au^{12}C^{16}O$)/2015 cm^{-1} ($Au^{13}C^{16}O$) (showing a site splitting at 2048/2003 cm^{-1}, respectively), one observes a quartet pattern of lines for the dicarbonyl at 1927.6, 1903.4, 1900.6, and 1833.0 cm^{-1}, the components of which have roughly equal intensities (cf. Figure 6A and B). Although partially overlapped by the gold monocarbonyl absorption, two of the weak in-phase CO stretching modes of the dicarbonyl were also observed at 2072 and 2024 cm^{-1} (cf. Figure 6A and B).

On the grounds that solid CO and N_2 are isomorphous under the 10-K conditions of our matrix experiments, we decided to investigate the $^{12}C^{16}O/^{13}C^{16}O/N_2$ reaction over an extended concentration range 1/1/1 to 1/1/200 in an attempt to further understand the origin of the inequivalence of the CO groups, that is, an isocarbonyl–carbonyl or a matrix perturbation effect. On varying the $^{12}C^{16}O/^{13}C^{16}O/N_2$ ratio from 1/1/1 to 1/1/200 one finds that the infrared spectrum remains essentially unchanged and, if anything, the resolution of the 1903.4/1900.6 cm^{-1} central doublet improves with increasing dilution as seen in Figure 8B. These experiments demonstrate that the inequivalence of CO groups is retained in both concentrated and dilute CO/N_2 matrices.

For an α-N_2 lattice which is very dilute in CO, it is difficult to conceive of any kind of lattice site effect that could reduce the symmetry of a normal dicarbonyl below that of the C_2 substitutional site. An asymmetrical C-bonded dicarbonyl, induced by a matrix perturbation, is therefore difficult to comprehend in an α-N_2 lattice.

On the other hand, attempts to rationalize the preference for an isocarbonyl–carbonyl complex in dilute CO/N_2 matrices are just as perplexing. One possibility is that, in CO/N_2 matrices, long-range dipole–dipole interactions between next-nearest-neighbor CO groups during the deposition–quenching process slightly favor the head-to-tail arrangement as found in the α-CO lattice.

Isotope Intensity Calculations for Isocarbonyl(carbonyl)gold. Using the best fit Cotton–Kraihanzel k_{CO}, k'_{CO}, and k_{CO-CO} force constants and the isotope intensity sum rules,[19,20] we calculated the relative intensities of the *eight* infrared-active CO stretching modes of the *four* isotopic molecules ($^nO^mC$)Au($^nO^mC$) ($m = 12$ or 13; $n = 16$). The observed and calculated intensities are listed in Table III. The agreement is acceptable, showing *four* intense (out-of-phase) low-frequency CO stretching modes with roughly equal absorbances and *four* much weaker (in-phase) high-frequency CO

Table III. Intensity and Frequency Calculations for ($^nO^mC$)Au($^nO^mC$) (Where n = 16 and m = 12 or 13)

Obsd freq, cm^{-1}	Intensities[a] Obsd	Calcd	Assignment
1927.7	~10	10.00	I
1905.4	~10	9.49	II
1901.5	~10	9.13	III
1885.3	~10	9.41	IV
~2072	~0.1	0.00	I
~2054	~1.6	0.65	II
~2050	~0.7	0.30	III
~2024	~0.2	0.15	IV

[a] The intensities were based on the isotope intensity sum rules[20] and a Cotton-Kraihanzel force field approximation[19] with k_{CO} = 15.88; k'_{CO} = 15.71, and k_{CO-CO} = 0.79 mdyn/Å.

Table IV. Vibrational Assignments for the CO Stretching Modes (cm^{-1}) of Au^{12}C^{16}O and Au^{13}C^{16}O

Matrix[a]	Au^{12}C^{16}O	Au^{13}C^{16}O
Ar	2039.4	1991.0
Kr	2040.5	1994.8
Xe	1985.5	1941.8

[a] The monocarbonyl shows a multiple trapping site effect at 2049.2/2001.2 cm^{-1} in Ar, 2064.5/2019.0 cm^{-1} in Kr, and 1970.9/1927.1 cm^{-1} in Xe for Au^{12}C^{16}O/Au^{13}C^{16}O, respectively. For the major sites in Ar, Kr, and Xe the C-K k_{CO} force constants are 16.81, 16.82, and 15.93 mdyn/Å, respectively.

stretching modes. It is gratifying that the intensity pattern calculated for the four components of the in-phase quartet (~0/0.65/0.30/0.15) is in qualitative agreement with the experimental isotope pattern (0.1/1.6/0.7/0.2) shown in Figure 6C and Table III.

Monocarbonyl Gold, AuCO. As mentioned earlier, when Au atoms are condensed with dilute Ar/CO, Kr/CO, and Xe/CO mixtures at 6–10 K, the infrared spectrum shows high-frequency CO stretching modes (besides those assigned to Au(CO)$_2$) at 2039.4, 2040.5, and 1985.5 cm^{-1}, respectively (Figures 2–4). In dilute Ne/CO = 1/10 to 1/100 matrices, the infrared spectra show the presence of only Au(CO)$_2$, presumably as a result of the higher mobility of Au atoms and CO molecules in Ne and poorer quenching efficiency of Ne compared to that of Ar, Kr, and Xe at 6–10 K.

On repeating the experiments in $^{12}C^{16}O/^{13}C^{16}O$/M matrices (M = Ar, Kr, Xe), the high-frequency absorption appeared as a doublet (Figures 2–4), establishing the identity of the monocarbonylgold complex beyond any doubt (Table IV).

The Elusive Gold Tricarbonyl. In this brief discussion we attempt to rationalize our inability to synthesize Au(CO)$_3$. If one examines the function $\Delta H_c = n\Delta F_{CO}$ (where ΔH_c has previously been shown[9] to be proportional to the enthalpy of decomposition of a series of related carbonyl complexes, M(CO)$_n$, and ΔF_{CO} is the change in the CO bond stretching force constant on passing from free to coordinated CO) for the group Cu(CO)$_{3,2,1}$ and Ag(CO)$_{3,2,1}$[2] and compares the values to those obtained for Au(CO) and Au(CO)$_2$ (Figure 9), one is forced to conclude that the gold carbonyl complexes are expected to be thermally less stable than their copper and silver counterparts. Moreover, the stability trends indicate that the elusive Au(CO)$_3$ complex would be thermally less stable than Ag(CO)$_3$ and Cu(CO)$_3$.

Our inability to synthesize Au(CO)$_3$ may therefore simply be the outcome of its thermal instability at the low temperatures employed.

Electronic Spectrum and Molecular Orbital Descriptions. (A) Bis(carbonyl)gold in Argon Matrices. The matrix uv–visible spectrum of Au(CO)$_2$ in concentrated CO/Ar ≃ 1/5 matrices displays an intense absorption (with superimposed

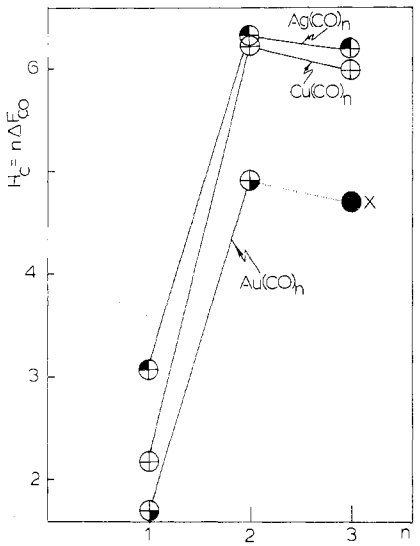

Figure 9. Graphical representation of the function $\Delta H_c = n\Delta F_{CO}$ vs. the coordination number n for the series of complexes M(CO)$_n$ (M = Cu, Ag, Au; n = 1–3). Note that the k_{CO} force constants used to evaluate ΔF_{CO} refer exclusively to the complexes in Ar matrices (see text and ref 9 for notation). The point marked X represents the estimated value of ΔH_c for the elusive Au(CO)$_3$ complex.

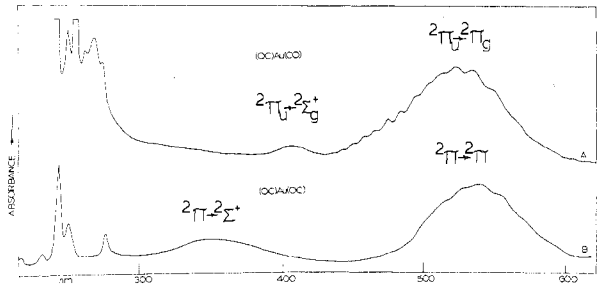

Figure 10. Uv-visible spectrum of Au atoms deposited with (A) a CO/Ar ≃ 1/5 mixture at 6–10 K and (B) pure CO at 6–10 K.

vibrational fine structure) in the visible region centered at roughly 520 nm (presumably responsible for the pronounced green color of Au(CO)$_2$), together with a weaker absorption at about 407 nm (Figure 10A).

(B) Isocarbonyl(carbonyl)gold in Carbon Monoxide Matrices. The matrix uv–visible spectrum obtained on cocondensing Au atoms with pure CO at 10 K shows an intense absorption in the visible region, centered at roughly 538 nm, and a weaker absorption at about 350 nm (Figure 10B). [In Figure 10A and B, high-energy transitions are observed in the region 280–200 nm and are probably best assigned to a mixture of atomic Au transitions and Au(CO)$_2$ and Au(CO)(OC) transitions. The presence of trace amounts of free gold atoms even in pure CO matrices provides another case of the subtle dependence of the product yield on the deposition temperature.[10] The relative amounts of atomic compared to molecular species are governed by the quenching rate compared to the complexation rate, quenching being favored at lower temperatures (6–10 K) and complexation at higher temperatures (15–20 K).] If this spectrum is in fact associated with (OC)Au(OC), as suggested from the corresponding infrared evidence, then the most noticeable difference between it and that for (OC)Au(CO) is the appreciable shift of the high-energy absorption from 407 to 350 nm (ca. 4000 cm^{-1}). On the other hand, the main absorption remains relatively unperturbed, shifting from 520 to 538 nm (ca. 640 cm^{-1}).

In an effort to try to understand these optical spectra and to gain an insight into the differences expected between a

Table V. Parameters Required to Reproduce the EHMO Calculations for (OC)Au(CO) and (OC)Au(OC)

	Orbital	Orbital exponent	H_{ii}, eV
Au	5d	4.025	−11.09
	6s	1.823	−9.22
	6p	1.823	−4.37
C	2s	1.608	−19.42
	2p	1.568	−10.64
O	2s	2.246	−32.33
	2p	2.227	−15.80

r(Au–C) = 2.11 Å; r(Au–O) = 2.07 Å; r(C–O) = 1.13 Å.

C-and O-bonded carbonyl, we have performed iterative extended Hückel calculations for the $D_{\infty h}$ symmetrical C-bonded dicarbonyl, the $C_{\infty v}$ asymmetrical C-bonded dicarbonyl, and the $C_{\infty v}$ isocarbonyl–carbonyl complex. The 5d, 6s, and 6p orbitals for Au and the 2s and 2p orbitals for C and O were employed in the calculations, with Clementi–Raimondi orbital exponents,[11] the Cusach approximation,[12] and Baetzold's values for the Coulomb integrals of Au.[13] The parameters required to reproduce these calculations are given in Table V. The resulting molecular orbital energy level schemes for (OC)Au(CO), (OC)Au(CO)*, and (OC)Au(OC) are shown in Figure 11.

One finds that the π back-bonding from the gold to the ligand (whether C or O bonded) appears to originate from both the (d_{xz}, d_{yz}) and to a larger extent, the (p_x, p_y) orbital sets of gold. The odd electron in both cases can be seen to reside in a degenerate Π_u molecular orbital which is mainly Au (p_x, p_y) in character.

It seems likely that the intense visible absorption at about 520 nm for (OC)Au(CO) and 538 nm for (OC)Au(OC) originates from a strongly allowed $^2\Pi_u \rightarrow {}^2\Pi_g$ electronic transition which, according to our scheme (Figure 11), should be relatively insensitive to the mode of CO coordination. On the other hand, the higher energy transition at roughly 407 nm for (OC)Au(CO) and 350 nm for (OC)Au(OC) could be associated with the strongly allowed $^2\Pi_u \rightarrow {}^2\Sigma_g^+$ transition, which is expected to be quite sensitive to whether the carbonyl is C or O bonded.

It is particularly noteworthy that the $^2\Pi_u \rightarrow {}^2\Pi_g$ transition involves transferring an electron from the Π_g (d_{xz}, d_{yz}) orbital which is *weakly* π bonding between the metal and the ligand and as such would be expected to depend little on the mode of coordination of the CO group, whereas the $^2\Pi_u \rightarrow {}^2\Sigma_g^+$ transition involves transferring an electron from a Σ_g^+ *strongly* σ-bonding orbital between the metal and ligand and would therefore be anticipated to show a larger perturbation with respect to CO linkage isomerism.

We also investigated the effect of gradually perturbing one of the Au–C bonds in (OC)Au(CO)*. In this EHMO calculation we systematically moved one of the CO groups away from the Au atom and examined the effect on the electronic levels as compared to the case of (OC)Au(CO). The first point to note is that a large (~1.5 Å) perturbation of the unique CO group is required in (OC)Au(CO)* to simulate the changes observed on simply switching one CO group around into the O-bonded configuration (Figure 11). Moreover, the calculated "sensitivity" of the high-energy transition compared to that of the low-energy transition turns out to be in the wrong direction for (OC)Au(CO)* but mirrors the observed trend for (OC)Au(OC) (although not in the right sense for either model).

One may therefore conclude that the differences between the optical spectra of Au atoms deposited with concentrated CO/Ar ≃ 1/5 and pure CO matrices are compatible with the $D_{\infty h}$ (OC)Au(CO) and $C_{\infty v}$ (OC)Au(OC) formulations proposed earlier on the basis of infrared isotopic data.

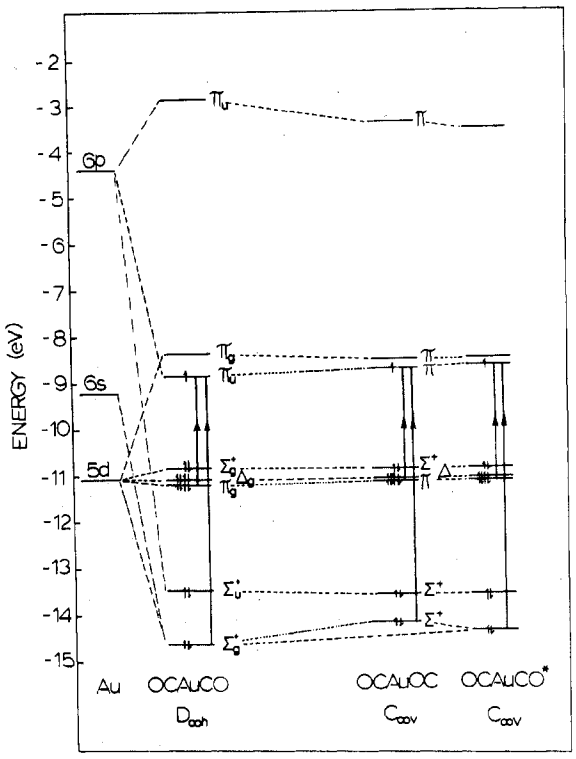

Figure 11. Quantitative molecular orbital energy level diagram for $D_{\infty h}$ Au(CO)$_2$, $C_{\infty v}$ Au(CO)(CO)*, and $C_{\infty v}$ Au(CO)(OC) based on the result of extended Hückel calculations (see text for parameters required to reproduce these calculations).

Matrix-Induced Vibrational Frequency Shifts for Bis(carbonyl)gold in Ne, Ar, Kr, Xe, CO, and N_2 Matrices. A study of vibrational frequency shifts for molecules in various solvents can sometimes provide useful information as to the nature of the solute–solvent interaction and as such can distinguish nonspecific interactions from weak chemical bonds. The theoretical interpretations of solute–solvent interactions have more recently been extended to include guest–host interactions for molecules, radicals, and ions trapped in solid matrices.[14] However, the detailed interpretation of a vibrational frequency shift from the gas phase to the matrix, defined as $\Delta\nu = \nu_{gas} - \nu_{matrix}$, is a complex calculation even for the simplest of systems and makes quantitative evaluation of matrix shifts impracticable. Providing the guest molecule is trapped within a "flexible" matrix cage, one would not expect its frequency shift behavior to differ markedly from the molecule in solution in the case of nonspecific guest–host interactions. Let us apply the Buckingham equation[15]

$$\frac{\Delta\nu}{\nu} = C_1 + {}^1/_2(C_2 + C_3)\left[\frac{\epsilon' - 1}{2\epsilon' + 1}\right]$$

which has been used with some success to explain nonspecific solvent shifts in $Co(CO)_n$ (where n = 1–4)[16] and $Ag(CO)_n$ (where n = 1–3),[2] to the case of $Au(CO)_2$ in various matrices.

Bis(carbonyl)gold has been studied in Ne, Ar, Kr, Xe, N_2, and CO. A monotonic red shift (a loose cage environment according to Pimentel and Charles[17]) is observed on passing from Ne to Ar to Kr to Xe matrices. The matrix frequencies for $Au(CO)_2$ in inert-gas matrices show an approximately linear dependence on the matrix polarizability (Figure 12). Extrapolation to zero polarizability yields the frequency 1931.3 cm^{-1}. We shall refer to this value as ν_{gas}, the "pseudo gas-phase frequency" for $Au(CO)_2$. Using the ν_{gas} value, one can determine the Buckingham frequency shift ratio $\Delta\nu/\nu$ (where ν is taken as the arithmetric mean of ν_{gas} and ν_{matrix}). The

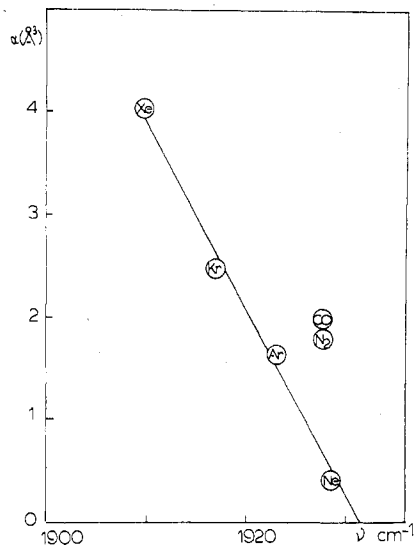

Figure 12. Polarizability (α, Å^3)–frequency (cm^{-1}) plot for the asymmetric CO stretching mode of $Au(CO)_2$ in Ne, Ar, Kr, and Xe matrices. (Points are also included for CO and N_2 matrices and refer to Au(CO)(OC)—see text.)

Table VI. Buckingham Frequency Plots for $Au(CO)_2$ in Ne, Ar, Kr, and Xe Matrices

Matrix	ν_{matrix}	$\Delta\nu$	$10^{-3}(\Delta\nu/\nu)^b$	$(\epsilon' - 1)/(2\epsilon' + 1)^c$
Ne	1928.6	2.70	1.399	0.130[d]
Ar	1923.0	8.30	4.307	0.148
Kr	1917.0	14.30	7.432	0.185
Xe	1909.7	21.60	11.247	0.221
Gas	1931.3[a]			

[a] Extrapolated value. [b] ν is the arithmetic mean frequency for the complex in the matrix and gas phase. [c] $\epsilon'_{20\ K} = 2.19$ (Xe), 1.88 (Kr), 1.63 (Ar). [d] $\epsilon'_{10\ K} = 1.51$ (Ne) (see text).

$\Delta\nu/\nu$ values are listed in Table VI and plotted against $(\epsilon' - 1)/(2\epsilon' + 1)$ in Figure 13, and they show a linear dependence for Ne, Ar, Kr, and Xe.

The excellent agreement for the Ne point in Figure 13 is gratifying as the ϵ' (10 K) has not previously been reported and the value for solid Ne was calculated from the mean of the extrapolated value of the $\Delta\nu/\nu$ vs. $(\epsilon' - 1)/(2\epsilon' + 1)$ plots for $Ag(CO)_3$[2] ($\epsilon'_{Ne} = 1.46$) and $Co(CO)_4$[16] ($\epsilon'_{Ne} = 1.56$) in Ar, Kr, and Xe matrices.

It would appear, therefore, that $Au(CO)_2$ interacts in a nonspecific manner with noble gas matrices. However, the frequencies for the dicarbonyl in solid CO and N_2 lie conspicuously off the plarizability–frequency plot by about 7–8 cm^{-1} and may be considered to be indirect support for the isocarbonyl–carbonyl formulation proposed earlier for Au atoms in solid CO and N_2 matrices.

Conclusion

In the inert-gas matrices Ne to Xe, there is little doubt that we have been able to generate, isolate, and identify the binary gold carbonyls Au(CO) and $Au(CO)_2$. However, the problem in pure CO and CO/N_2 matrices is more complicated, because one is inquiring whether or not an asymmetric C-bonded dicarbonyl can be distinguished from an isocarbonyl–carbonyl using vibrational and electronic spectroscopy.

Let us briefly collect the experimental and theoretical evidence as it presently stands with the aim of critically evaluating which model is favored.

1. The inequivalence of the CO groups is unambiguously depicted in $^{12}C^{16}O/^{13}C^{16}O$ and $^{12}C^{16}O/^{13}C^{16}O/N_2$ infrared experiments. This favors either model and incidentally indicates breakdown of the frequency-factored force field approximation.

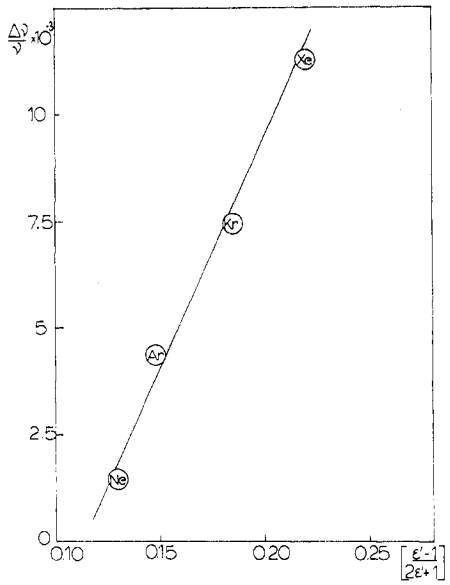

Figure 13. Buckingham plots for $Au(CO)_2$ in Ne, Ar, Kr, and Xe matrices.

2. The isotopic frequency of the $^{12}C^{18}O$-labeled molecule is higher than that of the $^{13}C^{16}O$-labeled molecule. On a simple mass basis, for a C-bonded carbonyl, this is an unexpected result. However, one would anticipate an unusual oxygen-18 shift if one of the carbonyl ligands was O bonded.

3. The observation of a relatively high infrared activity for the in-phase, high-frequency νCO stretching mode (2072 cm^{-1}) favors a "gross" inequivalence of the CO groups (Figure 5). The magnitude of this effect appears to be out of line with that anticipated for a small matrix perturbation effect, although not unreasonable for an isocarbonyl–carbonyl formulation.

4. Although ten isotopic molecules and their ν_{CO} frequencies have been observed, the nonobservation of the ν_{Au-C} modes renders the normal-coordinate calculations insensitive to distinguishing the two bonding models.

5. The ν_{CO} stretching frequencies in pure CO and CO/N_2 matrices are anomalous in a Buckingham sense (see Figure 12) but are consistent with either model.

6. The primitively related, next-nearest-neighbor CO groups around the C_2 substitutional site of solid CO are more compatible with the isolation of an isocarbonyl–carbonyl complex. The restrictions imposed by the head-to-tail arrangement of CO groups in a CO lattice could be responsible for the matrix stabilization of an isocarbonyl–carbonyl complex. It is difficult to conceive of any type of matrix perturbation effect that could render two C-bonded carbonyl groups inequivalent in a C_2 substitutional site. This point would argue in favor of the isocarbonyl model.

7. In α-N_2 matrices which are "isomorphous" with α-CO, isotope concentration experiments in the range $^{12}C^{16}O/^{13}C^{16}O/N_2 \simeq 1/1/1$ to $1/1/200$ demonstrate that a similar inequivalence of CO groups exists for the dicarbonyl. For an α-N_2 lattice which is very dilute in CO, it is difficult to imagine what kind of lattice site effect could reduce the symmetry of a normal dicarbonyl below that of the C_2 substitutional site. An asymmetrical C-bonded dicarbonyl, induced by a matrix perturbation, is therefore difficult to comprehend in an α-N_2 lattice.

On the other hand, attempts to rationalize the preference for an isocarbonyl–carbonyl complex in dilute CO/N_2 matrices are just as perplexing. One possibility is that long-range dipole–dipole interactions between CO groups during the deposition–quenching process slightly favor the head-to-tail

arrangement in the isomorphous α-N_2 lattice.

8. Finally, EHMO calculations performed on the asymmetrical C-bonded dicarbonyl and the isocarbonyl–carbonyl complex predict shifts in the uv–visible transitions of both complexes compared to the symmetrical C-bonded dicarbonyl. However, an unreasonably large (~1.5 Å) perturbation of the unique CO group is required in the asymmetrical C-bonded dicarbonyl to simulate the changes observed on simply switching one CO group into the O-bonded configuration.

Moreover, the sensitivity of the high-energy transition compared to the low-energy transition on passing from the symmetrical C-bonded dicarbonyl to the isocarbonyl–carbonyl (although not in the right direction—which is not unexpected within the limitations of EHMO theory) is at least consistent with the trend observed in practice. On the other hand, on passing from the symmetrical C-bonded dicarbonyl to the asymmetrical C-bonded dicarbonyl, the calculations predict the reverse trend; that is, the low-energy transition is more sensitive than the high-energy transition to the mode of CO bonding. The EHMO calculations therefore suggest that the isocarbonyl–carbonyl formulation is a more acceptable model than a lattice-perturbed asymmetrical C-bonded complex.

In conclusion we would argue that five out of the eight pieces of evidence lean toward the isocarbonyl–carbonyl formulation. However, our data are not unequivocal and other experiments will be required to unravel this fascinating yet perplexing chemical problem.

Acknowledgment. We thank the National Research Council of Canada, the Atkinson Foundation, and Liquid Carbonic for financial assistance and the National Research Council for a scholarship for D.M. We are also grateful to Mr. M. Peterson for supplying the SIMPLEX minimization subroutine used in our vibrational computations.

Registry No. ($^{16}O^{12}C$)Au($^{16}O^{12}C$), 60582-72-1; ($^{16}O^{12}C$)Au($^{16}O^{13}C$), 60582-73-2; ($^{16}O^{13}C$)Au($^{16}O^{12}C$), 60582-74-3; ($^{16}O^{13}C$)Au($^{16}O^{13}C$), 60582-75-4; ($^{16}O^{12}C$)Au($^{18}O^{12}C$), 60582-76-5; ($^{18}O^{12}C$)Au($^{16}O^{12}C$), 60582-77-6; ($^{18}O^{12}C$)Au($^{18}O^{12}C$), 60582-78-7; ($^{16}O^{12}C$)Au($^{18}O^{13}C$), 60582-79-8; ($^{18}O^{13}C$)Au($^{16}O^{12}C$), 60582-80-1; ($^{18}O^{13}C$)Au($^{18}O^{13}C$), 60582-81-2; Au($^{12}C^{16}O$), 60594-88-9; Au($^{13}C^{16}O$), 60594-89-0; $Au(CO)_2$, 60594-90-3.

References and Notes

(1) M. I. Bruce, *J. Organomet. Chem.*, **44**, 209 (1972).
(2) (a) H. Huber, E. P. Kündig, M. Moskovits, and G. A. Ozin, *J. Am. Chem. Soc.*, **97**, 2097 (1975); (b) D. McIntosh and G. A. Ozin, *ibid.*, **98**, 3167 (1976); (c) J. S. Ogden, *Chem. Commun.*, 978 (1971).
(3) E. P. Kündig, M. Moskovits, and G. A. Ozin, *J. Mol. Struct.*, **14**, 137 (1972).
(4) M. Moskovits and G. A. Ozin, *Appl. Spectrosc.*, **26**, 481 (1972).
(5) L. A. Hanlan and G. A. Ozin, *J. Am. Chem. Soc.*, **96**, 6324 (1974).
(6) H. Huber and G. A. Ozin, unpublished work.
(7) D. McIntosh and G. A. Ozin, in preparation.
(8) D. F. Shriver, *Chem. Br.*, **8**, 419 (1972).
(9) E. P. Kündig, D. McIntosh, M. Moskovits, and G. A. Ozin, *J. Am. Chem. Soc.*, **95**, 7234 (1973); M. Moskovits and G. A. Ozin in "Vibrational Spectra and Structure", J. Durig, Ed., Elsevier, Amsterdam, 1975; M. Moskovits and G. A. Ozin, *J. Mol. Struct.*, **32**, 71 (1976).
(10) T. A. Ford, H. Huber, W. Klotzbücher, and G. A. Ozin, *J. Am. Chem. Soc.*, **98**, 3176 (1976).
(11) E. Clementi and D. L. Raimondi, *J. Chem. Phys.*, **38**, 2686 (1963).
(12) L. C. Cusachs, *J. Chem. Phys.* **43**, 5157 (1965).
(13) R. Baetzold, *J. Chem. Phys.*, **55**, 4555 (1971).
(14) A. J. Barnes in "Vibrational Spectra of Trapped Species", H. Hallam, Ed., Wiley, London, 1973.
(15) A. D. Buckingham, *Proc. R. Soc. London, Ser. A.*, **248**, 169 (1958); **255**, 32 (1960); *Trans. Faraday Soc.*, **56**, 753 (1960).
(16) L. Hanlan, H. Huber, E. P. Kündig, B. McGarvey, and G. A. Ozin, *J. Am. Chem. Soc.*, **97**, 7054 (1975).
(17) G. C. Pimentel and S. W. Charles, *Pure. Appl. Chem.*, **7**, 111 (1963).
(18) J. K. Burdett, *Inorg. Chem.*, **14**, 375, 931 (1975); *J. Chem. Soc., Faraday Trans. 2*, **70**, 1599 (1974); M. Elian and R. Hoffmann, *Inorg. Chem.*, **14**, 1058 (1975).
(19) F. A. Cotton and C. S. Kraihanzel, *J. Am. Chem. Soc.*, **84**, 4432 (1962).
(20) E. B. Wilson, J. C. Decius, and P. C. Cross, "Molecular Vibrations", McGraw-Hill, New York, N.Y., 1955.

Contribution from Lash Miller Chemistry Laboratories and Erindale College, University of Toronto, Toronto, Ontario, Canada

Metal Atom Chemistry and Surface Chemistry. 1. Dioxygensilver, Ag^+,O_2^-, and Tetraoxygensilver, Ag^+,O_4^-, Reactive Intermediates in the Silver Atom–Dioxygen System. Relevance to Surface Chemistry

D. McINTOSH and G. A. OZIN*

Received May 11, 1976 AIC603450

The cocondensation reaction of Ag atoms with $^{16}O_2$ and $^{16}O_2$/Ar matrices at 6–12 K has been investigated by infrared and ultraviolet–visible spectroscopy. Dioxygen and silver concentration experiments, warm-up studies, and $^{16}O_2/^{18}O_2$ and $^{16}O_2/^{16}O^{18}O/^{18}O_2$ isotopic substitutions establish that two mononuclear complexes are formed which are best formulated as AgO_2 and AgO_4. The isotopic data suggest that the oxygen atoms in AgO_2 are equivalent and the uv–visible data imply the presence of an Ag^+,O_2^- ion pair. An ion-pair formulation is also arrived at for Ag^+,O_4^- by comparison with Ag^+,O_2^- as well as with the known alkali metal–dioxygen ion pairs Cs^+,O_2^- and Cs^+,O_4^-. The results for Ag/O_2 are found to be unique when compared with the available data for Cu/O_2 and Au/O_2 cocondensation reactions. The Ag/O_2 reaction products are further discussed in terms of their potential usefulness as localized bonding models for molecular dioxygen surface complexes which are known to participate in silver-catalyzed oxidation reactions.

Introduction

Molecular dioxygen surface species are of central interest in a variety of silver-catalyzed oxidation reactions.[1] Many of the mechanisms that have been proposed invoked $Ag(O_{2_{ads}})$ complexes as reactive intermediates rather than O^-_{ads} and/or O^{2-}_{ads} surface oxide species, all of which are known to coexist on freshly oxygenated silver films and supported silver catalysts.[1]

A potentially useful technique for gaining a localized bonding description[2] of metal–dioxygen surface interactions involves the isolation and spectroscopic study of the primary reaction products of metal atom–dioxygen matrix reactions. Previous studies of this type have led to the discovery of binary dioxygen complexes, MO_2 and O_2MO_2 (where M = Ni, Pd, Pt,[3] Rh,[4] Cr,[5] or Cu[5,6]), which would appear at this stage to be useful models for exploring the transient steps prior to dissociative chemisorption of dioxygen on metal surfaces.

In the context of the Ag/O_2 cocondensation reaction one would anticipate that AgO_2 would be one of the products. A complex of this type could possibly serve as a simple model